OPEN ACCESS
Applied Physics Express 18, 016506 (2025) LETTER
https://doi.org/10.35848/1882-0786/ada86b

AlScN/GaN HEMTs with 4 A/mm on-current and maximum oscillation frequency >130 GHz

Kazuki Nomoto[1*], Joseph Casamento[2], Thai-Son Nguyen[2], Lei Li[1], Hyunjea Lee[1], Chandrashekhar Savant[2], Austin Lee Hickman[1], Takuya Maeda[3], Jimy Encomendero[1], Ved Gund[2], Timothy Vasen[4], Shamima Afroz[4], Daniel Hannan[4], James C. M. Hwang[2], Debdeep Jena[1,2,3], and Huili Grace Xing[1,2,3]

[1]School of Electrical and Computer Engineering, Cornell University, Ithaca, NY 14853, United States of America
[2]Department of Materials Science and Engineering, Cornell University, Ithaca, NY 14853, United States of America
[3]Kavli Institute at Cornell for Nanoscale Science, Cornell University, Ithaca, NY 14853, United States of America
[4]Northrop Grumman Mission Systems Advanced Technology Laboratory, Linthicum, MD 21090, United States of America

*E-mail: kn383@cornell.edu

Received December 10, 2024; revised January 3, 2025; accepted January 8, 2025; published online January 27, 2025

Aluminum Scandium Nitride (AlScN) is an attractive material for use as a lattice-matched epitaxial barrier layer in GaN high-electron mobility transistors (HEMTs). Here we report the device fabrication, direct current (DC) and radio frequency (RF) characteristics of epitaxial AlScN/AlN/GaN HEMTs on SiC substrates with regrown ohmic contacts. These devices show record high on-current of over 4 A/mm, high cutoff frequency (f_T) of 92.4 GHz and maximum oscillation frequency (f_{MAX}) of 134.3 GHz.

High-performance radio frequency (RF) transistors with nitride semiconductors are used in a wide range of applications where high frequency,[1–3] low noise,[4,5] high linearity,[6] high power,[6,7] and reliability[8] are required. III-nitride HEMTs with AlGaN or InAl(Ga)N barrier layers enable high-power density at high frequencies for millimeter wave applications.[9–11] The large on-current densities result from the large 2-dimensional electron gas (2DEG) densities, which form due to polarization discontinuities at the heterojunction interface with GaN. The high electron mobility, a high breakdown field, and large thermal conductivity make nitride HEMTs leaders in high-power and high-frequency applications. These 2DEGs exhibit a much higher electron mobility than silicon inversion channels for higher speed, and simultaneously a wider energy bandgap than silicon for higher breakdown voltage.

Despite the impressive performances in recent years, several unresolved problems in III-nitride HEMTs restrict reaping the entire benefit from the intrinsic material properties. For high-power RF applications these problems are related to high gate leakage and current dispersion at higher frequencies. The high gate leakage current leads to decreased breakdown voltage, increased power dissipation, and reduced device reliability. The current dispersion limits gain these output power densities at larger frequencies. Several factors contribute to the gate leakage and current dispersion in GaN HEMTs, including high charge densities, electric field crowding, material defects, trap states, and surface states at the gate insulator/GaN interface. To address these concerns, various approaches are being investigated, such as improving the quality of the gate insulator/GaN interface, using passivation layers with high breakdown strength, and polarization-neutral device structures.[12,13]

Another way to address these concerns is by using new materials in the barrier layer. The gain and the speed of the transistor are related to its intrinsic transconductance $g_m, int \approx C_{gs,int} \times v_{sat}/L_g$, where $C_{gs,int} = \varepsilon \times L_g \times W_g/d$ is the intrinsic gate-source capacitance, $\varepsilon = \epsilon_0 K$ is the dielectric constant of the barrier material and K the relative dielectric constant, d is its thickness, and v_{sat} is the electron saturation velocity in the electron channel. Decreasing d is necessary when L_g is scaled to prevent short channel effects, but this also increases the gate leakage current exponentially via Fowler Nordheim tunneling,[14,15] which decreases the breakdown voltage. High-K material gate insulator results in a desired larger gate capacitance, while reducing the gate leakage by allowing a thicker d, reducing the electric field and therefore the gate leakage. *In situ* grown epitaxial high-K dielectrics are ideal from this point of view since they potentially eliminate chemical impurities and structural defects at the gate and channel interface.

For GaN HEMTs, aluminum scandium nitride (AlScN) is such a high-K gate insulator[16,17] which has high thermal and chemical stability, and offers the option of lattice matching with GaN.[18,19] The use of *in situ* high-K AlScN gate barrier GaN HEMTs offers hope for the above advantages to simultaneously enhance intrinsic transconductance and breakdown voltage, akin to the metal-high K gate stack in the Si MOSFETs, as well as curb the interfacial states.

In this work, HEMTs made from AlScN/AlN/GaN heterostructures are studied. The DC and RF characteristics of unpassivated HEMTs with various gate lengths are investigated, with 90 nm gate length devices showing large on-current densities up to 4 A/mm and on/off ratios greater than 10^3 despite relatively low room temperature electron mobilities (494 $cm^2/V \cdot s$) in these devices. Previous reports demonstrate the promising device performance of scaled AlScN-GaN HEMTs,[20–22] and these results expand on those by showing the largest on-current densities (4A/mm) reported to date. These large on-current densities are partially facilitated by the relatively small source-drain distance of 600 nm in the scaled devices in this study. With expected future improvements in electron mobility and heterostructure design to enhance transconductance, these results demonstrate the great potential of AlScN to improve the output power and maximum speed of nitride based millimeter wave integrated circuits.

Figure 1(a) shows the GaN/$Al_{0.86}Sc_{0.14}N$/AlN/GaN HEMT structure, which consists of a 2 nm GaN cap layer, a 5 nm $Al_{0.86}Sc_{0.14}N$ barrier, a 2 nm AlN spacer (total barrier thickness: 9 nm), a 1000 nm unintentionally doped GaN channel, and AlN nucleation layer on a 10 × 10 mm^2 6H semi-insulating SiC substrate, grown by plasma assisted molecular beam epitaxy (PA-MBE). Figure 1(b) shows an AFM image of as-grown surface of GaN/$Al_{0.86}Sc_{0.14}N$/AlN/GaN HEMT structure. The corresponding root means square (RMS) roughness is 1.171 nm for an AFM scan area of 10 × 10 μm^2. Room temperature Hall-effect measurements with In-dots prior to device fabrication showed a 2DEG sheet concentration of $\sim 3 \times 10^{13}$ cm^{-2} and electron mobility of 494 $cm^2/V \cdot s$, corresponding to a sheet resistance of 417 Ω/sq. Figure 1(a) also shows the regrown n^+ GaN source/drain ohmic contacts schematic of the AlScN/AlN/GaN HEMT device. The device fabrication process started with patterning of a SiO_2/Cr mask for n^+GaN ohmic regrowth by PA-MBE. The pre-regrowth etch depth into the HEMT structure was 40 nm, and regrown n^+GaN was 100 nm with a Si doping level of 7×10^{19} cm^{-3}. Non-alloyed ohmic contacts of Ti/Au were deposited by e-beam evaporation. T-shaped Ni/Au (30/350 nm) gates were formed by electron-beam lithography, followed by liftoff. Transmission line measurements (TLM) yielded an average contact resistance of 0.31 $\Omega \cdot$ mm. The device presented here has a regrown n^+GaN source-drain distance L_{sd} of 600 nm, a gate width of 2 × 25 μm, and a gate length L_g of 90 nm. An SEM image of completed AlScN/AlN/GaN HEMT is shown in Fig. 1(c) with the zoomed-in view of the gate shown in Fig. 1(d).

Room temperature Hall-effect measurements on Van der Pauw test structures on the same die as the HEMT devices in this paper show a 2DEG sheet concentration of 2.20×10^{13} cm^{-2} and electron mobility of 494 $cm^2/V \cdot s$, corresponding to a sheet resistance of 573 Ω/sq. These values allow for the performance of these HEMTs to be evaluated but do not represent the lowest sheet densities that are possible in these heterostructures. In a previous study, room temperature electron mobilities exceeded 1500 cm^2 $V \cdot s$ in a similar heterostructure by Casamento et al.[17] The mobility of our sample (494 $cm^2/V \cdot s$) is reasonable considering the unoptimized GaN buffer growth on 6H-SiC thus the interface roughness near where the 2DEG resides in this study. The lower mobility compared to prior works, can also be attributed to the higher sheet charge density ($\sim 3 \times 10^{13}$ cm^{-2}) observed in our samples arising from a higher Sc composition. This higher charge density contributes to an enhanced device output current, even though it increases scattering effects, which slightly reduces mobility. The tunability of AlScN properties in terms of strain balance and ferroelectricity affords a wide range of potential applications.[23] As demonstrated in recent studies,[24] with judiciously chosen Sc content, AlScN/AlN/GaN heterostructures can be strain balanced in the device structure while exhibiting excellent polarization properties, strong 2DEG confinement and reliable device operation. Integration of heterostructures and fabrication of devices with lower sheet resistances will be the subject of future work.

The following device results were obtained using a Keithley 4200 semiconductor characterization system for DC, and an Agilent Technologies E8364B network analyzer for RF characteristics. For RF characterization, scattering parameters were measured from 50 MHz to 50 GHz, and calibrated using short, open, load, and through impedance standards on an alumina substrate. The parasitics were de-embedded using fabricated open and short test structures on the same sample.

Figure 2(a) shows representative family $I-V$ curves of the device, measured for $V_{ds} = 0$ to 6 V and $V_{gs} = 4$ to -10 V. The device has a maximum drain current $I_{dMAX} = 4.07$ A/mm and an on-resistance R_{on} of 0.59$\Omega \cdot$mm is extracted at $V_{gs} = 0$ V. The transfer curves are shown in Fig. 2(b). A peak transconductance g_m of 0.50 S/mm is obtained at $V_{ds} = 5$ V. The transfer characteristics were measured after the output characteristics and showed a decrease in maximum on-current densities from approximately 4 to 2.1 A/mm. This decrease in current density for scaled devices and ultra-thin barrier layers

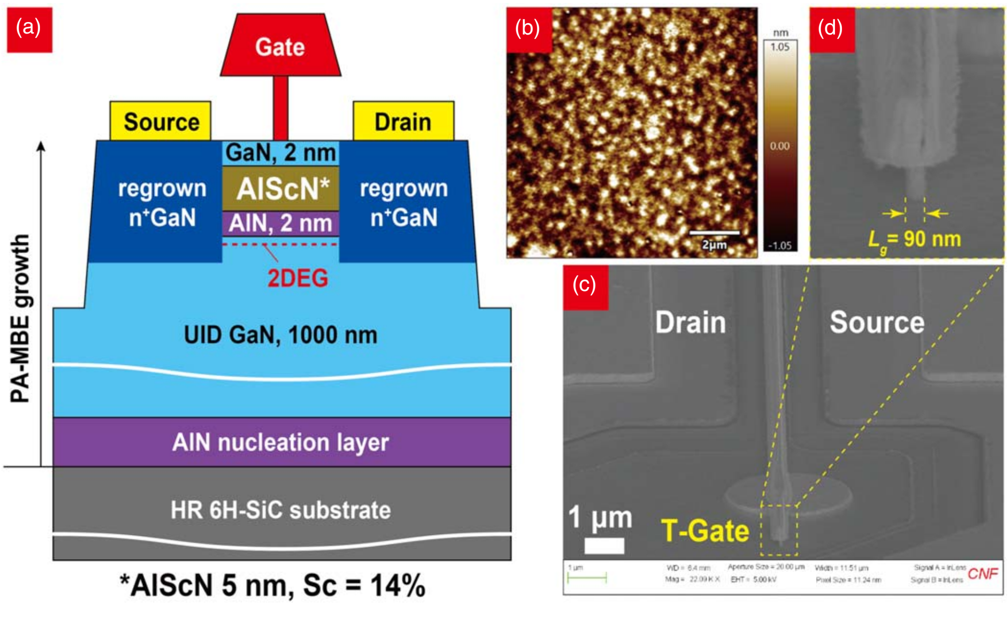

Fig. 1. (a) Cross Sect. schematic for the GaN HEMT with regrown contacts, and the high-K AlScN layer in the barrier layer is 5 nm thick. (b) AFM image of the as-grown sample surface. (c) SEM image of a processed HEMT, and (d) inset shows the zoomed-in image of a T-gate.

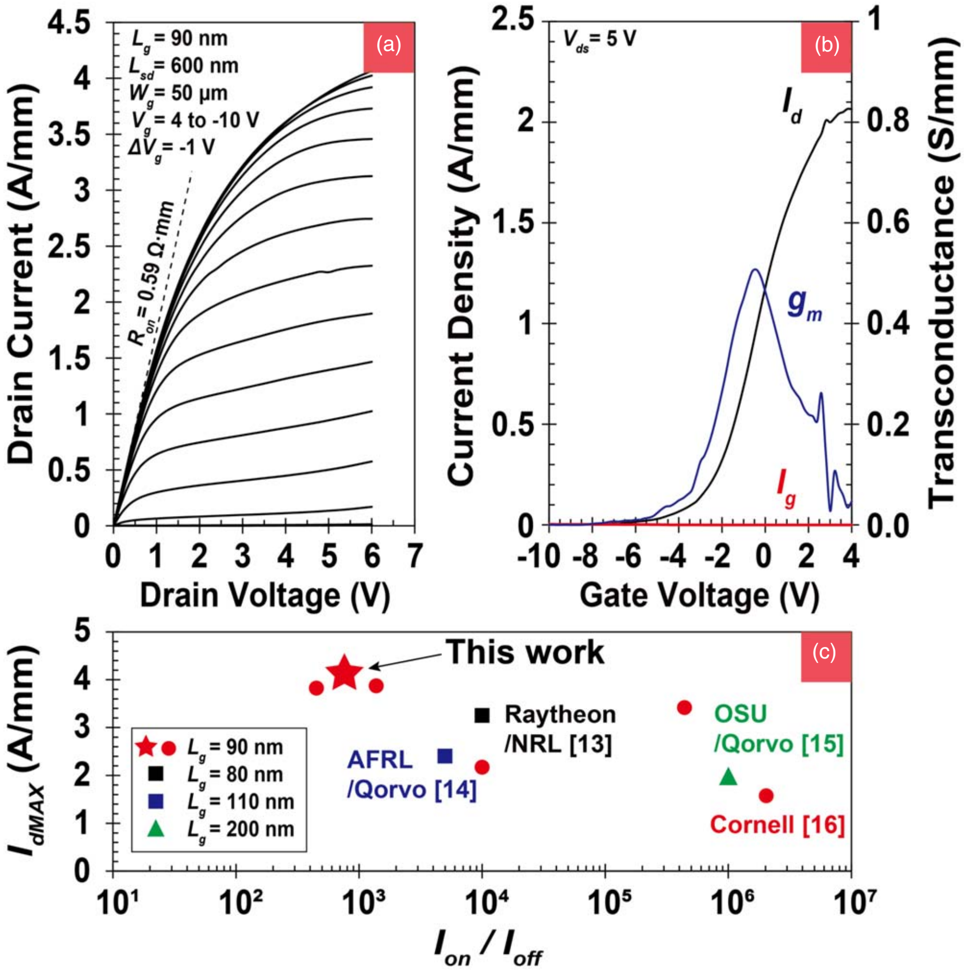

Fig. 2. (a) Family $I-V$ curves and (b) transfer characteristics of the device with $L_g = 90$ nm and $L_{sd} = 600$ nm. (c) Output current benchmark of AlScN HEMTs with previous reports.[25–28]

after several measurement cycles is not unexpected since the devices were not passivated. Figure 2(c) benchmarks the AlScN barrier GaN HEMTs of this work with earlier reports[25–28] of $Al_xSc_{1-x}N$/Al(Ga)N/GaN HEMTs. All AlScN barrier GaN HEMTs show high output currents compared to conventional GaN HEMTs with AlGaN or InAl(Ga)N barriers with similar device designs. This is due to the larger polarization discontinuity of AlScN with GaN thus a high channel charge.[17,23,29,30]

Figure 3(a) shows the current gain $|H_{21}|^2$ and unilateral gain U of the AlScN barrier HEMT as a function of frequency at the peak f_T bias condition, $V_{ds} = 6$ V, and $V_{gs} = -1$ V. The extrapolation of both $|H_{21}|^2$ and U with -20 dB/dec slope gives the current gain cutoff frequency/maximum oscillation frequency f_T/f_{MAX} of 92.4/134.3 GHz after de-embedding. Figures 3(b) and 3(c) show the bias-dependence heat maps of the f_T/f_{MAX} values extracted in the same manner as Fig. 3 (a) at various V_{gs} and V_{ds}. The heat maps indicate that the highest RF performance of the AlScN/GaN HEMT is achieved at an on-current of 3.13 A/mm at $V_{ds} = 6$ V.

Figure 4 shows the three terminal off-state breakdown measurements with various gate-drain distances (L_{gd}). The breakdown voltage does not scale linearly with L_{gd}, as expected, which is caused by the non-uniform distribution of the electric field within the channel. Among all devices, the highest breakdown voltage observed is $BV = 78$ V ($L_{gd} = 3.85$ μm), corresponding to an average electric field of 0.2 MV/cm. During the measurement and prior to breakdown, the gate current is found to be roughly equal to the drain current. This indicates that the off-state drain current and breakdown is dominated by gate-drain leakage, not avalanche or channel breakdown, and is far from intrinsic material limits. The breakdown mechanism appears to be a hard breakdown. This is evidenced by the inability of the device to recover post-breakdown and visible structural damage under optical inspection. The damage is predominantly observed around the gate and drain electrode edges, as these regions are subject to the highest electric field intensities during device operation. Capacitance-voltage (C-V) measurements (not shown) in these heterostructures show a relative dielectric permittivity of $\kappa = 15$ for the 5-nm AlScN barrier, similar to high-k values reported in thicker AlScN samples.[16] However, the lower than expected breakdown voltage indicates the high-K aspect of AlScN is not manifested in the device performance. Typically, AlN-GaN RF HEMTs show breakdown electric fields upwards of 1–2 MV/cm.[7] This points to room for improvement in the insulating behavior of the AlScN layer. Nevertheless, to explore the potential for high-frequency applications, the breakdown behavior of submicron channel length devices was examined. An average breakdown voltage of 35.5 V was measured for a device with a 455 nm gate-drain distance. This corresponds to an effective breakdown field of 0.78 MV/cm. Based on these results, the Johnson's figure-of-merit (JFOM =

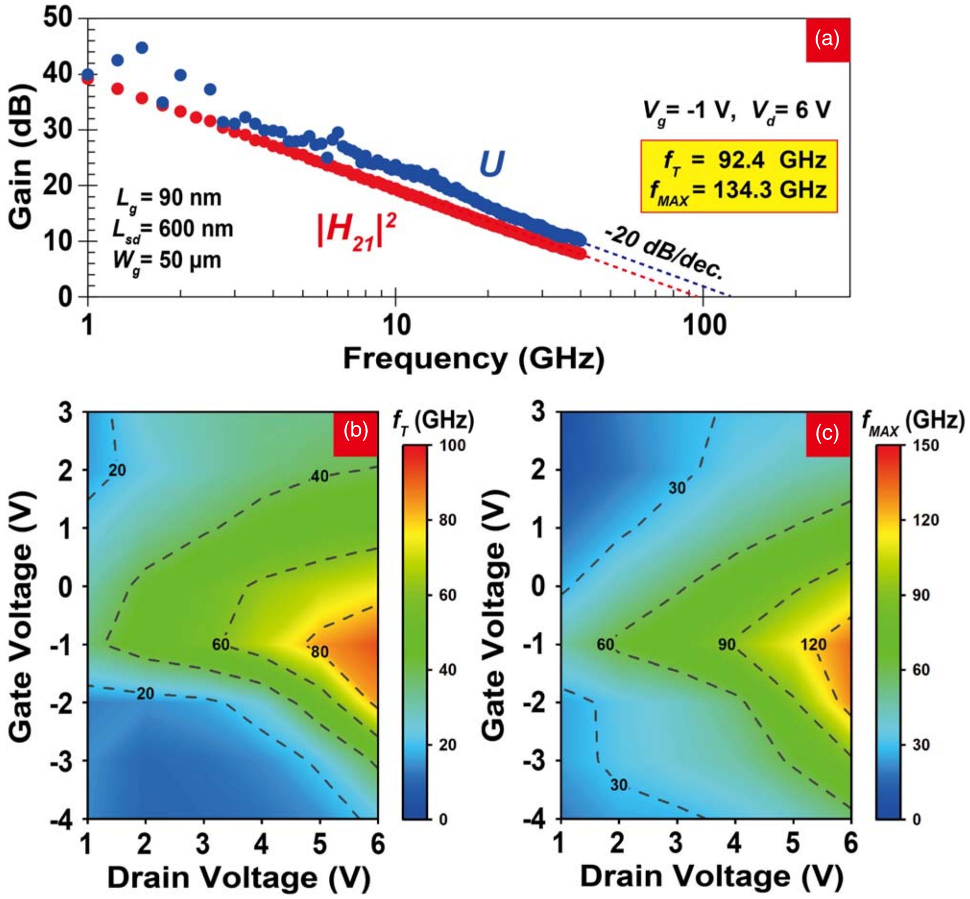

Fig. 3. (a) Current gain and unilateral gain of the device with $L_g = 90$ nm, showing $f_T/f_{\mathrm{MAX}} = 92.4/134.3$ GHz. A gain decay of -20 dB/dec is plotted with the dash lines to show f_T and f_{MAX} extrapolation. V_{ds} and V_{gs} bias dependence of (b) f_T and (c) f_{MAX} extracted from U. The colors indicate frequencies on the contour maps.

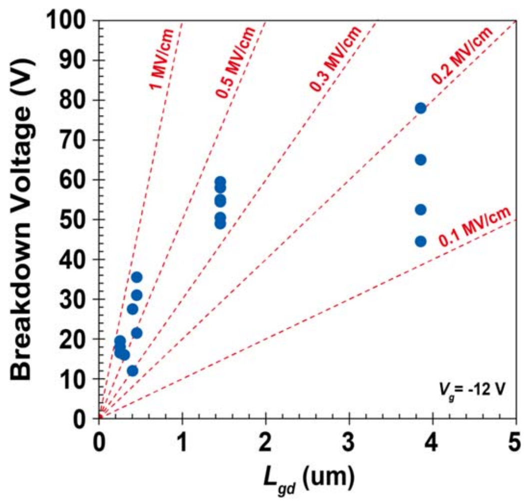

Fig. 4. Breakdown voltage scaling as a function of gate-drain separation ranging from 0.25 to 3.85 μm. The gate length of all measured devices is 90 nm.

$f_T \times BV$) of the fabricated AlScN HEMT is $\sim$1.8 THz · V. Future breakdown voltage values may also be improved by introducing a passivation process to minimize contribution from surface states and a field plating process to manage the electric field distribution on the gate-drain side.

In summary, epitaxial AlScN barrier HEMTs with an AlN interlayer deliver record high on-current of over 4 A/mm in spite of a modest channel sheet resistance of 573 Ω/sq. Simultaneously, a high cutoff frequency (f_T) of 92.4 GHz and maximum oscillation frequency (f_{MAX}) of 134.3 GHz is obtained, leading to a JFOM greater than 1 THz · V. This heterostructure demonstrates an ongoing effort to integrate the promising physical properties of AlScN with existing III-nitride HEMT technology.

Acknowledgments This work was supported, in part, by Northrop Grumman Mission Systems university research funding. This work was also supported, in part, by the SRC and DARPA through the Joint University Microelectronics Program (JUMP) 2.0, and performed at the Cornell NanoScale Facility, an NNCI member supported by the NSF under Grant No. NNCI-2025233.

Data availability

The data that supports the findings of this study is available from the corresponding author upon reasonable request.

ORCID iDs Jimy Encomendero https://orcid.org/0000-0002-1597-1761

1) L. Li et al., "GaN HEMTs on Si with regrown contacts and Cutoff/Maximum oscillation frequencies of 250/204 GHz," IEEE Electron Device Lett. **41**, 689 (2020).
2) H. W. Then et al., "Scaled submicron field-plated enhancement mode high-K gallium nitride transistors on 300mm Si(111) wafer with power FoM (RON xQGG) of 3.1 mohm-nC at 40V and fT/fMAX of 130/680 GHz," 2022 International Electron Devices Meeting (IEDM), 35.1.1 (2022).
3) Y. Tang, K. Shinohara, D. Regan, A. Corrion, D. Brown, J. Wong, A. Schmitz, H. Fung, S. Kim, and M. Micovic, "Ultrahigh-speed GaN high-electron-mobility transistors with $f_T/f_{\max}$ of 454/444 GHz," IEEE Electron Device Lett. **36**, 549 (2015).
4) M. Glória Cao de Andrade, L. Felipe de Oliveira Bergamim, B. Baptista Jnior, C. Roberto Nogueira, F. Alex da Silva, K. Takakura, B. Parvais, and E. Simoen, "Low-Frequency noise investigation of AlGaN/GaN high-electron-mobility transistors," Solid-State Electron. **183**, 108050 (2021).

5) S.-S. Yang and Y.-M. Hsin, "Low-frequency noise characterization of AlGaN/GaN HEMTs with and without a p-GaN gate layer," Semicond. Sci. Technol. **36**, 125021 (2021).
6) K. Shinohara et al., "(Invited) GaN-based multiple 2DEG channel BRIDGE (Buried Dual Gate) HEMT technology for high power and linearity," ECS Trans. **92**, 103 (2019).
7) A. Hickman, R. Chaudhuri, L. Li, K. Nomoto, S. J. Bader, J. C. M. Hwang, H. G. Xing, and D. Jena, "First RF power operation of AlN/GaN/AlN HEMTs with >3 A/mm and 3 W/mm at 10 GHz," IEEE J. Electron Devices Soc. **9**, 121 (2021).
8) M. Meneghini et al., "GaN-based power devices: physics, reliability, and perspectives," J. Appl. Phys. **130**, 181101 (2021).
9) S. Wu, X. Ma, L. Yang, M. Mi, M. Zhang, M. Wu, Y. Lu, H. Zhang, C. Yi, and Y. Hao, "A millimeter-wave AlGaN/GaN HEMT fabricated with transitional-recessed-gate technology for high-gain and high- linearity applications," IEEE Electron Device Lett. **40**, 846 (2019).
10) A. Shanbhag, F. Grandpierron, K. Harrouche, and F. Medjdoub, "Physical insight of thin AlGaN back barrier for millimeter-wave high voltage AlN/GaN on SiC HEMTs," Appl. Phys. Lett. **123**, 142102 (2023).
11) S. Piotrowicz et al., "InAlGaN/GaN with AlGaN back-barrier HEMT technology on SiC for Ka-band applications," International Journal of Microwave and Wireless Technologies **10**, 3946 (2018).
12) S. Yang, Z. Tang, M. Hua, Z. Zhang, J. Wei, Y. Lu, and K. J. Chen, "Investigation of SiNx and AlN passivation for AlGaN/GaN high-electron-mobility transistors: role of interface traps and polarization charges," IEEE J. Electron Devices Soc. **8**, 358 (2020).
13) R. Chaudhuri, A. Hickman, J. Singhal, J. Casamento, H. G. Xing, and D. Jena, "In-situ crystalline AlN passivation for reduced RF dispersion in strained-channel AlN/GaN/AlN high-electron-mobility transistors," Physica Status Solidi (a) **219**, 2100452 (2022).
14) J. Robertson, "High dielectric constant gate oxides for metal oxide Si transistors," Rep. Prog. Phys. **69**, 327 (2005).
15) C.-H. Lee, S.-H. Hur, Y.-C. Shin, J.-H. Choi, D.-G. Park, and K. Kim, "Charge-trapping device structure of SiO2/SiN/high-k dielectric Al_2O_3 for high-density flash memory," Appl. Phys. Lett. **86**, 152908 (2005).
16) J. Casamento et al., "Epitaxial ScxAl1-xN on GaN exhibits attractive high-K dielectric properties," Appl. Phys. Lett. **120**, 152901 (2022a).
17) J. Casamento, T.-S. Nguyen, Y. Cho, C. Savant, T. Vasen, S. Afroz, D. Hannan, H. G. Xing, and D. Jena, "Transport properties of polarization-induced 2D electron gases in epitaxial AlScN/GaN heterojunctions," Appl. Phys. Lett. **121**, 192101 (2022b).
18) T.-S. Nguyen, N. Pieczulewski, C. Savant, J. J. P. Cooper, J. Casamento, R. S. Goldman, D. A. Muller, H. G. Xing, and D. Jena, "Lattice-matched multiple channel AlScN/GaN heterostructures," APL Mater. **12**, 101117 (2024).
19) L. van Deurzen, T.-S. Nguyen, J. Casamento, H. G. Xing, and D. Jena, "Epitaxial lattice-matched AlScN/GaN distributed Bragg reflectors," Appl. Phys. Lett. **123**, 241104 (2023).
20) E. M. Chumbes, J. Logan, B. Schultz, M. DeJarld, M. Tahhan, N. Kolias, M. Hardy, M. Ancona, and D. Meyer, "ScAlN-GaN transistor technology for Millimeter-wave ultra-high power and efficient MMICs (2022 IEEE/MTT-S International Microwave Symposium - IMS, 2022) p. 295.
21) S. Krause, I. Streicher, P. Waltereit, L. Kirste, P. Brckner, and S. Leone, "AlScN/GaN HEMTs grown by metal-organic chemical vapor deposition with 8.4 W/mm output power and 48% power-added efficiency at 30 GHz," Electron Device Letters **44**, 17 (2023).
22) M. B. Tahhan, J. A. Logan, M. T. Hardy, M. G. Ancona, B. Schultz, B. Appleton, T. Kazior, D. J. Meyer, and E. M. Chumbes, "Passivation schemes for ScAlN-Barrier mm-Wave high electron mobility transistors," IEEE Trans. Electron Devices **69**, 962 (2022).
23) M. Yassine, A. Yassine, A. Nair, B. Sundarapandian, N. Afshar, L. Kirste, S. Fichtner, and O. Ambacher, "Modeling of polarization reversal-induced interface sheet charge in wurtzite-type AlScN/GaN heterostructures," J. Appl. Phys. **135**, 155702 (2024).
24) T. S. Nguyen, K. Nomoto, W. Zhao, C. Savant, H. G. Xing, and D. Jena, "Strain-balanced AlScN/GaN HEMTs with f_T/f_{MAX} of 173/321 GHz," 2024 International Electron Devices Meeting (IEDM), 9.5.1 (2024).
25) T. E. Kazior, E. M. Chumbes, B. Schultz, J. Logan, D. J. Meyer, and M. T. Hardy, "High power density ScAlN-based heterostructure FETs for mm-Wave applications," 2019 IEEE MTT-S International Microwave Symposium (IMS), 1136 (2019).
26) A. J. Green et al., "ScAlN/GaN high-electron-mobility transistors With 2.4-A/mm current density and 0.67-S/mm transconductance," IEEE Electron Device Lett. **40**, 1056 (2019).
27) J. Cheng et al., "Breakdown voltage enhancement in ScAlN/GaN high-electron-mobility transistors by High-k bismuth zinc niobate oxide," IEEE Trans. Electron Devices **68**, 3333 (2021).
28) J. Casamento et al., "FerroHEMTs: high-current and high-speed all-epitaxial AlScN/GaN ferroelectric transistors," 2022 International Electron Devices Meeting (IEDM), 11.1.1 (2022).
29) O. Ambacher, B. Christian, M. Yassine, M. Baeumler, S. Leone, and R. Quay, "Polarization induced interface and electron sheet charges of pseudomorphic ScAlN/GaN, GaAlN/GaN, InAlN/GaN, and InAlN/InN heterostructures," J. Appl. Phys. **129**, 204501 (2021).
30) O. Ambacher, A. Yassine, M. Yassine, S. Mihalic, E. Wade, and B. Christian, "Electron accumulation and distribution at interfaces of hexagonal ScxAl1-xN/GaN- and ScxAl1-xN/InN-heterostructures," J. Appl. Phys. **131**, 245702 (2022).